

## Design study of plasma control system on JT-60SA for high beta operation

M. Takechi 1), G. Matsunaga 1), G. Kurita 1), S. Sakurai 1), H. Fujieda 1), S. Ide 1), N. Aiba 1), T. Bolzonella 2), A. Ferro 2), L. Novello 2), E. Gaio 2), F. Villone 3) and JT-60SA Team

1) Japan Atomic Energy Agency, Naka, Ibaraki 311-0193 Japan

2) Consorzio RFX, Padova, Italy

3) Cassino Univ. , Cassino, Italy

E-mail contact of main author: takechi.manabu@jaea.go.jp

**Abstract.** One of the important missions of JT-60SA is to demonstrate and develop steady-state high beta operation in order to supplement ITER toward DEMO. Specifications of plasma control system including the stabilizing plate, the RWM control coils, the error field correction coils and fast position control coils were determined based on simulations and expected plasma regime. Full non-inductive steady-state plasma with  $\beta_N = 4.3$  at  $I_p = 2.3$  MA will be achieved with these control systems. Simulation of plasma disruption was also performed to evaluate design values of Electro Magnetic forces of components.

### 1. Introduction

To achieve a steady-state high beta plasma, suppression of RWM is especially necessary because no-wall beta limit of steady state plasma with a large bootstrap current fraction is relatively low due to low internal inductance. There are two procedures for RWM stabilization. One is stabilization by plasma rotation and the other is that by feedback control with active coils. Stabilization by plasma rotation is preferable to that by use of in-vessel coils from the point of view of technical issues. However, it is recently reported that RWM is sometimes triggered by ELM, Fishbone, Energetic particle driven Wall Mode and so on even with sufficient rotation [1]. Therefore, we prepare RWM control coils (RWMCs) in the vacuum vessel for JT-60SA, in order to achieve steady-state high beta plasma and also to clarify stabilization mechanism of RWM to be extrapolated toward ITER and DEMO. For RWM stabilization, error field correction is necessary because error field destabilize RWM by reducing plasma rotation and resonant field amplification. Therefore, we will install error field correction coils (EFCCs) in the vacuum vessel. Of course, error field correction will play important role for plasma break down and avoidance of locked mode. EFCC will be also used for ELM control. JT-60SA has full super conducting coil system for toroidal field coils and poloidal field coils. It is difficult to control fast plasma position and to stabilize vertical instability by using only the super conducting poloidal field coils. Therefore, fast plasma position control coils (FPCCs) will be installed for control of vertical instability and plasma position.

In this paper, we show the plasma control system with in-vessel coils on JT-60SA. Figure 1 shows the in-vessel components.

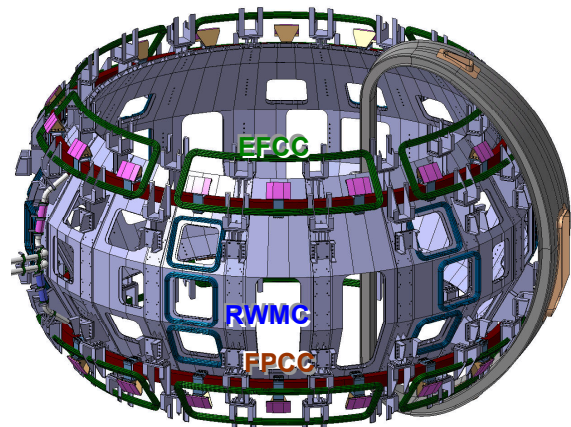


Fig. 1 Drawings of in-vessel components, Stabilizing plate (SP), fast position control coils (FPCC), resistive wall mod control coil (RWMC) and error field correction coil (EFCC).

## FT/P6-30

RWMCs, EFCCs and FPCCs are drawn with the stabilizing plate. After this introduction, RWM control is explained in section 2. The error field control system is shown in section 3 with ELM control. The fast plasma control system is shown in section 4 with simulation of plasma position control. The disruption simulation is necessary for design of in-vessel coils and also for other JT-60SA components. Therefore halo current, eddy current and so on has been evaluated and reported in section 5. Discussion and the summary are given in section 6.

### 2. Steady state high beta plasma with RWM control system.

We have surveyed the plasma conditions for full non-inductive plasma current drive and high beta ( $\beta_N > 4.0$ ) with ACCOME code and MARG2D code [2]. Figure 2 shows an example of the plasma profiles at  $I_p = 2.3$  MA with  $\beta_N = 4.3$  calculated with ACCOME code. We found by MARG2D code that this equilibrium is stable for  $n \leq 4$  kink-ballooning mode with ideal wall.

Active coils will be installed on the stabilizing plate at the opposite side from the plasma for control of RWM with  $n \leq 3$  control as shown Fig. 1. RWM system consists of three coils in the poloidal direction and six coils in the toroidal direction, therefore total coil number is eighteen. Each RWMC has eight-turns conductors. The stabilizing plate has SS316L double wall with 10mm thickness respectively and decreases the growth rate of vertical instability and RWM to the time scale of the wall, therefore we can control them by feed back systems with FPCCs and RWMCs. RWM control simulations are performed with VALEN code, which consist of MHD stability code and feed back simulation with three dimensional structure of vacuum vessel, stabilizing plate, coils and so on. These simulations show that high beta close to the ideal-wall limit ( $C_\beta = (\beta_N - \beta_N^{\text{no-wall}}) / (\beta_N^{\text{ideal-wall}} - \beta_N^{\text{no-wall}}) = 0.9$ ) is expected [3]. From the FEM analysis [4], we have determined the thickness and material of sheath of RWMC conductor.

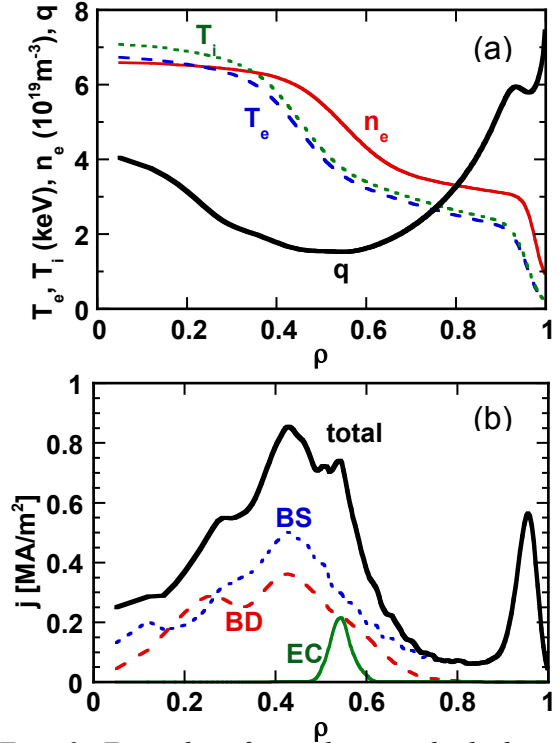


Fig. 2 Example of steady-state high beta plasma, (a) Profiles of ion temperature ( $T_i$ ), electron temperature ( $T_e$ ), electron density ( $n_e$ ) and safety factor ( $q$ ). (b) Current profile of boot strap (BS), beam driven (BD), electron cyclotron (EC) and OH

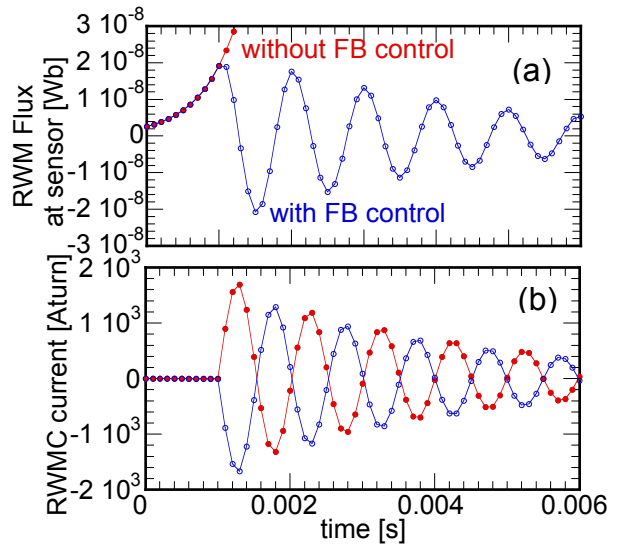


Fig. 3 Time evolution of RWM amplitude at the magnetic sensor without (red) and with (blue) FB control (a) and RWM currents at different positions (b).

## FT/P6-30

We will use 1mm SS316L sheath for the conductor. Requirements of coil current and voltage are evaluated by VALEN results and FEM analysis. The RWMC current requirement was estimated with time domain VALEN simulation for the plasma with  $\beta_N = 4.2$  corresponding to  $C_p = 0.9$  as shown in Fig. 3. FB starts at  $t = 0.001$  s and RWM is stabilized (Fig. 3 (a)). It is found from Fig. 3 (b) that the RWMC current requirement is  $\sim 1.7$ kAT. However, in VALEN simulation the conductor does not have sheath and stabilizing plate has single wall configuration, while conductor has stainless steel sheath and stabilizing plate has double wall configuration for current design. Therefore effects induced from these differences have been evaluated with FEM analysis. It is found that induced magnetic field at 1kHz for current configuration is about 6 times smaller than that of VALEN model. From these results, we have evaluated the requisite current 20kAT for RWM control with reasonable time delay. Figure 4 shows the impedance of RWMC and voltage at the coil with 20kAT calculated by FEM analysis. We need about 300V for RWM control shown as figure 3, because we will control RWM up to 1kHz. We need additional voltage of about 50V for coil feeders, therefore, we adopt the voltage requirement as 400V of RWM amplifiers for the present RWMC design.

### 3. Error field correction and ELM control

Error field correction is important for plasma initiation, avoidance of locked mode and RWM control. Therefore, we prepare EFCC on the vacuum vessel as shown Fig. 1. EFCC system consists of two coils in the poloidal direction and six coils in the toroidal direction, therefore total coil number is twelve. Maximum allowable error field is adopted as  $B_{pen} / B_t \sim 2 \times 10^{-4}$  for JT-60SA from the point of view of locked mode avoidance. Where,  $B_{pen}$  is the error field penetration threshold for  $m/n = 2/1$  locked mode defined as [5],

$$B_{pen}^2 = B_{r2,1}^2 + 0.8B_{r3,1}^2 + 0.2B_{r1,1}^2.$$

$B_{r,m,n}$  shows the harmonic component of  $m/n$  error field. Stray field from the canceling coil of the NBI have to be considered as source of error field especially for JT-60SA because the NBI system is close to the poloidal field coils compared with other tokamak systems e.g. JT-60U and ITER. NB system feel large magnetic field from poloidal

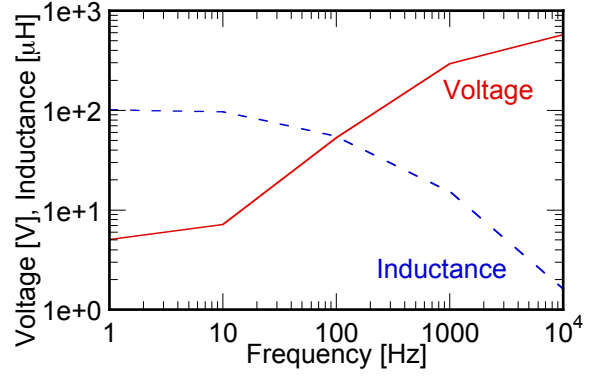


Fig. 4 Voltage and Inductance versus frequency of RWMC calculated with FEM analysis.

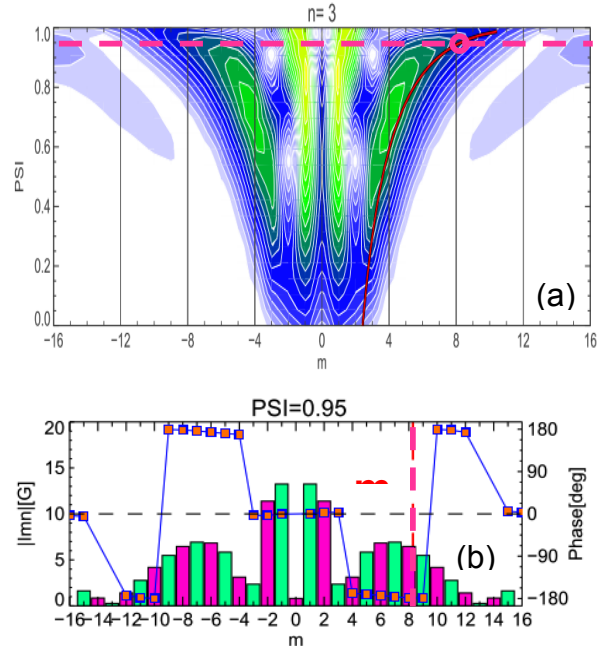


Fig. 5 (a) Contor plot of the poloidal fourior component of  $n=3$  EFCC induced magnetic field in the JT-60SA plasma. Red solid line shows the  $m=3q$  with  $n=3$  at each plasma position. (2) Magnitude and Phase of poloidal component at  $q_{95}$  shown with broken pink line in Fig 4 (a) with 30kAT EFCC. Vertical pink line shows the poloidal mode number at  $q_{95}$ .

## FT/P6-30

field coils, which should be canceled or reduced at NBI. If we use the huge ferromagnetic body surrounding NBI system in order to reduce the magnetic field from poloidal coils at beam splitting area, unacceptable large error field is induced at plasma region. Therefore, we will use active coil and reasonable amount of ferromagnetic body for canceling the magnetic field at NBs. We evaluated the stray field, which is induced by poloidal coils and plasma current, at NBs for the considerable plasma scenario for evaluation of the maximum canceling coil current of NBs. By using this maximum current, the error field penetration threshold due to stray field from NB canceling coil has been evaluated  $B_{pen} \sim 1$  G. Error field caused from the misalignment of the poloidal and toroidal coils has been calculated from presumed tolerance of the poloidal and toroidal coils with statistical approach. From these evaluation, EFCC current of  $\sim 20$  kAT is required.

The EFCC will be used for ELM control with Resonant Magnetic Perturbation (RMP) procedure [6]. In the case of  $n=3$  and up-down in-phase configuration, RMP field from the EFCC can resonant with magnetic field line as shown in Fig 5 (a). For example, resonant magnetic fourier component is about 6G ( $m=8$ ) at  $q_{95}$  with 30 kAT of EFCC current as shown in Fig 5 (b).

### 4. Simulation of plasma control with fast position control coils

Two FPCCs, each of which consists of 24 turns conductor with 120kAT, will be installed as shown in Fig. 1. Controllability of plasma position with FPCC is studied for vertical instability, ELM and mini collapse. The feed back plasma position control simulation has been performed with the linearized Grad-Shafranov equation and 3D FEM analysis [7]. FPCCs are able to control plasma position fast and reduce current and voltage requirement of the superconducting poloidal field coils from several thousand – several 10 thousand Voltage to several

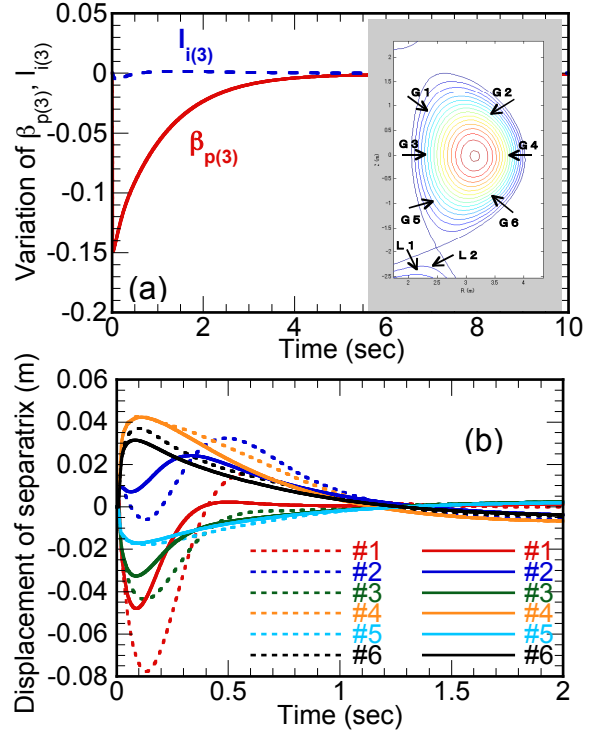


Fig. 6 (a) Time evolution of variation of  $\beta_{p(3)}$  (red solid line) and  $l_{i(3)}$  (blue broken line) used for plasma position control simulation. (b) Time evolution of displacement of separatrix, each position of which is shown in (a), without (dotted lines) and with (solid lines) horizontal control.

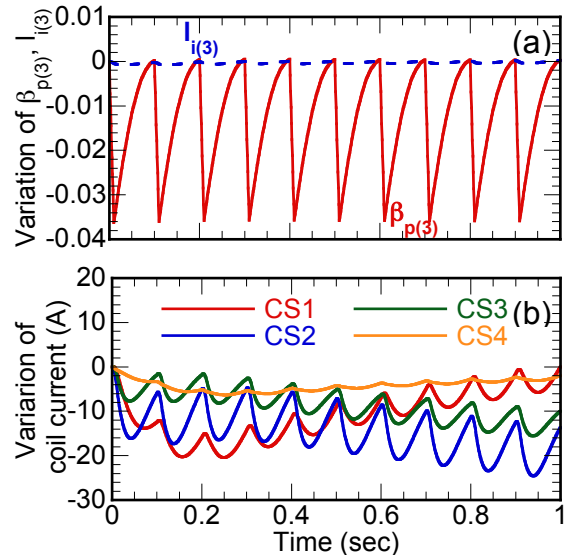


Fig. 7 Time evolution of variation of  $\beta_{p(3)}$  (red solid line) and  $l_{i(3)}$  (blue broken line) used for plasma position control simulation with ELM (a) and variation of CS coil current. (b)

## FT/P6-30

hundred Voltage for the vertical instability stabilization. Each FPCC coil has individual power supply in order to induce vertical magnetic field for horizontal position control. Simulation of past plasma position control with and without horizontal position control has been performed for mini collapse with 20 % drop of  $\beta_p$  for the 5.5MA plasma with  $\beta_{p(3)} = 0.74$  and  $l_{i(3)} = 0.70$ . Each FPCC coil has individual power supply for the case with horizontal control. FPCCs are connected in series and have opposite current direction for the case without horizontal control. Maximum displacement of separatrix with horizontal control is reduced by about half and recovers to the original position faster compared with those without horizontal control as shown in Fig. 6 (b). Also Maximum variation of poloidal coil current is found to be reduced by about half of that without horizontal control.

Simulation of the fast plasma position control with ELM has been performed for AC loss evaluation of superconducting coils. The ELM frequency of 10 Hz and 5% drop of  $\beta_p$  are assumed for the simulation (Fig 7 (a)). The current variation and voltage of poloidal coils, (Fig. 7 (b) for EF coils), FPCCs and eddy current of the stabilizing plate and the vacuum vessel are evaluated from this simulation and we estimate the magnetic field variation at PF coils for AC loss calculation.

## 5. Disruption simulation

### 5.1. Disruption simulation and Halo current

Disruption simulations with DINA code [8] are performed for calculations of (1) halo current for evaluation of EM load of vacuum vessel, (2) over current of PF coils for design of coils and power supplies and evaluation of AC loss of PF coils (3) EM force of the FPCC (4) eddy current of the vacuum vessel and stabilizing plate. DINA code calculates free boundary plasma equilibria, taking into account eddy currents in the vacuum vessel and a model of the power supplies. We performed three type of disruption simulation. First is Downward VDE Disruption, second is Upward VDE Disruption and third is Major Disruption (MD). VDE is caused by vertical instability due to loss of control. We have assumption for VDE simulation as (a) Disruption (thermal quench) starts at  $q_{\text{edge}}=1.5$ . (b) Current quench starts, after 0.5 ms from thermal quench. (c) Plasma Current decreases linearly in 10 ms and 30 ms. As for MD, Plasma stays at center when disruption (thermal quench) starts. For MD simulation, we have assumptions as (d) current quench starts 0.5 ms after thermal quench, (e) plasma current decreases linearly in 4 ms. The vacuum vessel and stabilizing plate is modeled by a set of thin plates with relevant resistance, so that the global  $L/R$  time can be

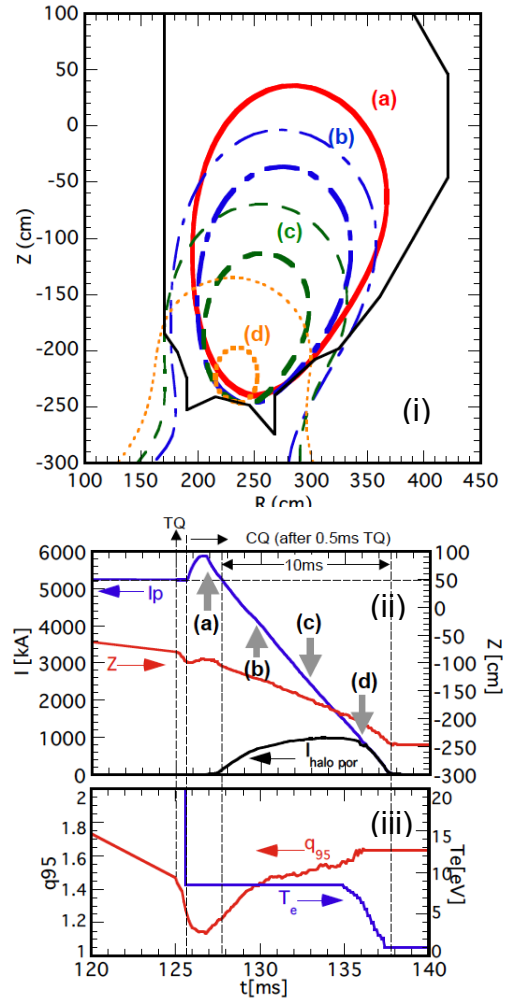


Fig. 8 (i) Plasma movement during downward VDE. Temporal evolution of  $I_p$  (blue), vertical position of current center (red) and poloidal halo current (black) (ii) and  $T_e$  (blue) and  $q_{95}$  (red) (iii). Alphabets in Fig. (ii) show the time of the plasma cross-section drawn in Fig. (i).

## FT/P6-30

matched with that calculated for the actual geometry. As for boundary, Coordinates of the plasma facing line are determined as a limiter of a plasma by the first wall and the divertor. As the initial plasma for DINA simulation we adopted the plasma equilibrium at end of burn with maximum current 5.5MA with  $\beta_{p(3)} = 0.83$  and  $I_{i(3)} = 0.71$ . All coils are supposed to be short-circuited. Figure 8 shows the example of the simulation results for downward VDE with current quench time  $\tau_{CQ} = 30$  ms. Plasma moves downward from  $t = 0$  ms and  $q_{95}$  decreases because of reduction of plasma surface. After that, thermal quench occurs at  $q_{95} = 1.5$ . Current quench starts 0.5ms after thermal quench. Electron temperature decrease rapidly at thermal quench and is tuned artificially in order for linear decrease of plasma current with  $\tau_{CQ} = 30$  ms. Halo current emerges after the plasma halo region contact at the first wall. Maximum halo current is evaluated 1.3MA for downward VDE with current quench time  $\tau_{CQ}=30$ ms as shown in Figure 8 (b). By using this value and waveform, the machine components have been designed. Poloidal halo current is larger with longer  $\tau_{CQ}$  and this result is same as that done for ITER [9].

### 5.2. Over current of PF coils at disruption

For design of PF coils and the power supply of PF coils and evaluation of AC loss of superconducting coils, calculation of maximum current of PF coils is necessary. Induced current at disruption of all PF coils are in the same direction as plasma current. However, Initial current of All CSs, EF1, EF2, EF6 coils at disruption are opposite in sign to plasma current, therefore absolute value of current of them decrease after disruption. On the other hand, absolute value of current of EF3, EF4, EF5 increase at disruption. Maximum over current of them is  $\sim 1.3$ kA for EF5 as shown in Fig. 9. It means that if we use EF5 with maximum rated current of 20kA, the current reach to 21.3kA at disruption. These results are used for design of PF coils and protection circuit of power supply. We have performed the simulation for VDE and MD with various current quench time, and found that induced current are little affected by change of direction of disruption, difference of current quench time and also difference of initial current of PF coils because of the large shielding effect of the vacuum vessel.

### 5.3. EM force of FPCC at disruption

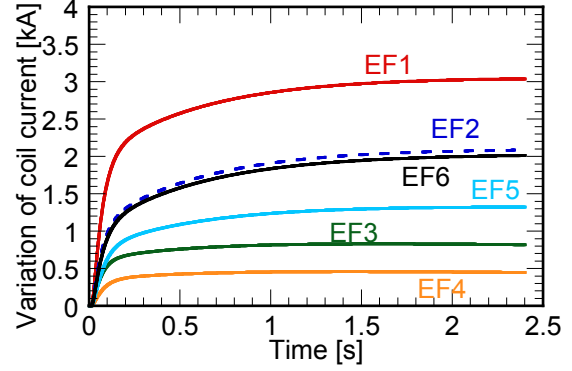


Fig. 9 Time evolution of variation of EF coil current at major disruption (MD) with  $\tau_{CQ} = 4$  ms. Only EF3-5 has positive current at disruption, therefore maximum over current is  $\sim 1.3$ kA of EF5.

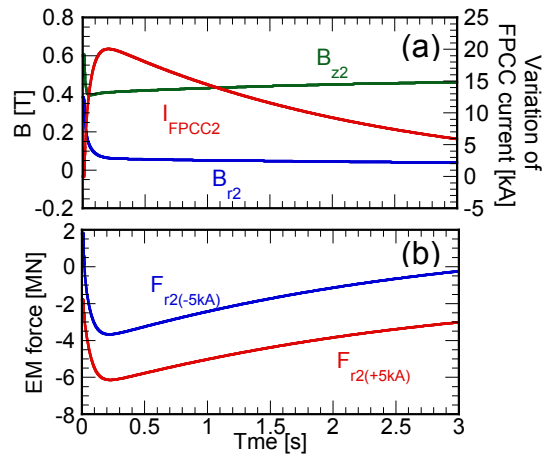


Fig. 10 (a) Time evolution of variation of the lower FPCC coil current (red),  $B_r$  (blue) and  $B_z$  (green) at lower FPCC during major disruption (MD) with  $\tau_{CQ} = 4$  ms. (b) Time evolution of EM force of lower FPCC. Maximum rated value  $\pm 5$ kA is added as initial current to FPCC current.

## FT/P6-30

For design of vacuum vessel and FPCC, evaluation of EM force of FPCC at disruption is necessary. EM force calculations of FPCC with 16 turns and 24 turns have been performed with DINA code and the circuit equation code during VDE and MD with various current quench time. Figure 10 shows the case of maximum EM force for FPCC with 24 turns. Time evolution of EM forces during major disruption (MD) with  $\tau_{CQ} = 4$  ms are shown with variation of the lower FPCC coil current and magnetic field at lower FPCC. Maximum rated value  $\pm 5$  kA is added as initial current to FPCC current. Although difference of turn number is 1.5 times, maximum EM force of FPCC with 24 turns is at most 1.2 times larger than that with 16 turns, because maximum FPCC current for 24 turns is only 70-75% of that for 16 turns due to larger inductance with 24 turns. We have decided the turn number of FPCC as 24 turns and have designed with these results.

## 6. Discussion and summary

The specifications of in-vessel coils, i.e. RWMC, EFCC and FPCC, for steady-state high beta operation have been determined by using the several simulations. We have evaluated the specification of RWMC with VALEN simulation and FEM analysis. Though mode-rigidity of RWM is assumed in these simulations, it is not known actually if RWM is rigid or not. The problem of mode-rigidity is very important for JT-60SA, because the coverage area of plasma with coils is very small as shown in Fig. 1. We have begun to perform the experiments for the study of mode-rigidity on RFX devices with reduced sets of coils. RFX has 192 coils, which cover whole plasma surface, with independent 192 amplifiers and successfully controls RWMs [10]. We try to control RWM with reduced sets of coils and study the effect of sideband effect and mode deformation. We have performed the feed back simulation of fast plasma position control with FPCC for determination of specification of FPCC and also for evaluation of AC loss of superconducting coils. For design of vacuum vessel, EF and CS coil, amplifier of the coils, FPCC and so on, disruption simulations with DINA code for the case of VDE and MD with various current quench time have been performed.

## References

- [1] G. Matsunaga *et al.*, Phys. Rev. Lett. **103**, 045001 (2009).
- [2] Y. Kamada, *et al.*, this conference, FTP/P6-04.
- [3] T. Fujita *et al.*, Nucl. Fusion **47** 1512–1523 (2007).
- [4] A. Ferro *et al.*, to be submitted to Fusion Eng. Des.
- [5] ITER Physics Basis, Nucl. Fusion **47** S128-S202 (2007).
- [6] T.E. Evans *et al.*, Phys. Rev. Lett. **92**, 235003-1 (2004).
- [7] I. Senda *et al.*, Nucl. Fusion **42** 568–580 (2002).
- [8] R.R. Khayrutdinov, V.E. Lukash, Journal of Comp. Physics **109** 193 (1993)
- [9] M. Sugihara *et al.*, Nucl. Fusion **47** 337–352 (2007).
- [10] T. Bolzonella *et al.*, Fusion Eng. Des. **82**, 1064 (2007).